Hot electron diffusion, microwave noise, and piezoresistivity in Si from first principles

Benjamin Hatanpää and Austin J. Minnich*

Division of Engineering and Applied Science, California Institute of Technology, Pasadena, California 91125, USA

(Received 4 October 2023; revised 16 April 2024; accepted 13 May 2024; published 3 June 2024)

Ab initio calculations of electron-phonon interactions in materials without adjustable parameters have provided microscopic insights into their charge-transport properties. Other transport properties such as the diffusion coefficient provide additional microscopic information and are readily accessible experimentally, but few *ab initio* calculations of these properties have been performed. Here, we report first-principles calculations of the hot electron diffusion coefficient in Si and its dependence on electric field over temperatures from 77–300 K. While qualitative agreement in trends such as anisotropy at high electric fields is obtained, the quantitative agreement that is routinely achieved for low-field mobility is lacking. We examine whether the discrepancy can be attributed to an inaccurate description of f-type intervalley scattering by computing the microwave-frequency noise spectrum and piezoresistivity. These calculations indicate that any error in the strength of f-type scattering is insufficient to explain the diffusion coefficient discrepancies. Our findings suggest that the measured diffusion coefficient is influenced by factors such as space-charge effects, which are not included in *ab initio* calculations, impacting the interpretation of experimental measurements in terms of microscopic charge-transport processes.

DOI: 10.1103/PhysRevB.109.235201

I. INTRODUCTION

Ab initio calculations of linear transport coefficients such as the electrical mobility of materials without adjustable parameters are now routine [1–5]. The approach is based on density-functional theory (DFT) and density-functional perturbation theory (DFPT) to compute the electronic structure, phonons, and electron-phonon matrix elements, followed by Wannier interpolation to the fine grids needed for transport calculations [6,7]. Transport properties are obtained by solving the Boltzmann equation with the collision matrix computed from the *ab initio* inputs. The accuracy of these calculations for low-field mobility has been established for many materials, including Si [1,2,8], GaAs [4,5,8], and others [9].

High-field transport properties, as well as noise properties such as the power spectral density (PSD) of current fluctuations, are also experimentally accessible and provide additional information about microscopic transport phenomena [10,11]. For instance, intervalley noise, in which carrier number fluctuations between valleys are observable as current fluctuations, can only be observed in a multivalley semiconductor such as n-Si [10,12]. The PSD of hot electrons in Si has been experimentally investigated at a range of frequencies, temperature, and electric-field strengths. Measurements of the electron-diffusion coefficient (proportional to low-frequency PSD) at room temperature along the [111] direction indicated a pronounced decrease with increasing electric field [13]. A subsequent study at lower temperatures showed an initial increase of the diffusion coefficient with increasing field, followed by the decrease seen at higher temperatures [14]. A clear anisotropy in the diffusion coefficient was observed between the [100] and [111] directions for high electric fields ($\gtrsim$2 kV cm^{-1}) across 77–300 K [14], despite the cubic symmetry of Si, and was attributed to intervalley noise. The frequency dependence of the PSD at low temperatures ~80 K was also examined, showing how thermal, convective, and intervalley noise contribute at different frequencies for these two directions [15].

Despite extensive experimental investigation, transport and noise properties beyond the low-field regime have historically been evaluated using semiempirical Monte Carlo methods [14,16–18]. These models utilized various approximations, such as dispersionless optical phonons, Debye acoustic phonons, and model band structures. More recently, the Monte Carlo method in n-Si has been extended to device simulation [19] and full-band studies [20–23]. Computations of high-field transport properties using *ab initio* methods have only recently been reported [24–28]. In GaAs, the drift velocity characteristics up to several kV cm^{-1} have been computed and have provided evidence for the role of two-phonon scattering [26,27]. The warm electron tensor of n-Si, including two-phonon scattering, has also been computed and directly compared to experiment [29]. An *ab initio* formalism to calculate fluctuational properties like PSD has also been developed recently [24]. Previous studies have used the formalism to compute the electric-field dependence of the PSD in p-Si [28] and n-GaAs, in the latter case including two-phonon scattering [26,27]. However, whether *ab initio* methods can accurately account for hot electron transport and noise properties in n-Si has not yet been determined.

Here, we report first-principles calculations of the hot electron diffusion coefficient and frequency-dependent PSD

*Corresponding author: aminnich@caltech.edu

 ©2024 American Physical Society

in *n*-Si, including two-phonon scattering. We find that although some qualitative features of the diffusion coefficient are correctly predicted, such as an anisotropy at high electric fields, quantitative agreement is in general poor. To identify the origin of the discrepancies, we computed the microwave-frequency PSD and piezoresistivity. The computed properties are in reasonable qualitative agreement, constraining the magnitude of inaccuracy in the computed intervalley scattering rate. Together, these observations indicate that the diffusion coefficient discrepancies may be attributed to factors which are not included in the *ab initio* formulation of charge transport, for instance real-space gradients and space-charge effects. This finding has relevance to the interpretation of diffusion coefficient measurements in terms of microscopic charge-transport processes.

II. THEORY AND NUMERICAL METHODS

Our approach to solve for the high-field transport and noise properties of charge carriers has been described previously [24,26,28,29]. In brief, for a spatially homogeneous, nondegenerate electron gas subject to an applied electric field, the Boltzmann transport equation (BTE) is given by

$$\frac{q\mathbf{E}}{\hbar}\cdot\nabla_{\mathbf{k}}f_{\mathbf{k}} = -\sum_{\mathbf{k}'}\Theta_{\mathbf{k}\mathbf{k}'}\Delta f_{\mathbf{k}'}. \tag{1}$$

Here, q is the carrier charge, $\mathbf{E}$ is the electric field vector, $f_{\mathbf{k}}$ is the distribution function describing the occupancy of the electronic state indexed by wavevector $\mathbf{k}$, $\Delta f_{\mathbf{k}'}$ is the perturbation to the equilibrium electron distribution function $f^0_{\mathbf{k}}$, and $\Theta_{\mathbf{k}\mathbf{k}'}$ is the linearized collision matrix given by Eq. (3) of Ref. [24]. We assume that only one band contributes to charge transport and thus neglect the band index. This formulation of the BTE is applicable to arbitrarily high fields for nondegenerate electrons as shown in Ref. [26].

For sufficiently large electric fields, the reciprocal space derivative of the total distribution function must be evaluated numerically. In the present formulation, the derivative is computed using a finite-difference approximation given in Refs. [30,31]. The BTE then takes the form of a linear system of equations (Eq. (5) in Ref. [24]) that can be solved by numerical linear algebra:

$$\sum_{\mathbf{k}'}\Lambda_{\mathbf{k}\mathbf{k}'}\Delta f_{\mathbf{k}'} = \sum_{\gamma}\frac{qE_\gamma}{k_BT}v_{\mathbf{k},\gamma}f^0_{\mathbf{k}}. \tag{2}$$

Here, E_γ and $v_{\mathbf{k},\gamma}$ are the electric field and electron drift velocity along the γ-Cartesian axis, and the relaxation operator $\Lambda_{\mathbf{k}\mathbf{k}'}$ is defined as

$$\Lambda_{\mathbf{k}\mathbf{k}'} = \Theta_{\mathbf{k}\mathbf{k}'} + \sum_{\gamma}\frac{qE_\gamma}{\hbar}D_{\mathbf{k}\mathbf{k}',\gamma}, \tag{3}$$

where $D_{\mathbf{k}\mathbf{k}',\gamma}$ is the momentum-space derivative represented in the finite-difference matrix representation given by Eq. (24) in Ref. [30]. The BTE is solved using numerical linear algebra to obtain the steady-state electron distribution function, from which transport properties can be obtained using an appropriate Brillouin zone sum. For instance, the drift velocity in the β direction is given by

$$V_\beta = \frac{1}{N}\sum_{\mathbf{k}}v_{\mathbf{k},\beta}f_{\mathbf{k}}, \tag{4}$$

where $N = \sum_{\mathbf{k}}f_{\mathbf{k}}$ is the number of electrons in the Brillouin zone. Similarly, the mobility is given by

$$\mu_{\alpha\beta}(\mathbf{E}) = \frac{2e^2}{k_{\mathbf{B}}T\mathcal{V}_0}\sum_{\mathbf{k}}v_{\mathbf{k},\alpha}\sum_{\mathbf{k}'}\Lambda^{-1}_{\mathbf{k}\mathbf{k}'}\left(v_{\mathbf{k}',\beta}f^0_{\mathbf{k}'}\right), \tag{5}$$

where $\mathcal{V}_0$ is the supercell volume, α is the direction along which the current is measured, and β is the direction of the applied electric field [1]. Once mobility is found at different stresses, the inverse (normalized to zero stress) yields the piezoresistivity.

The fluctuations in the occupancy of electronic states manifest in experiment as current noise, which can be characterized by the power spectral density (PSD). As derived in Ref. [24], the current PSD $S_{j_\alpha j_\beta}$ can be calculated at a given angular frequency ω as

$$S_{j_\alpha j_\beta}(\omega) = 2\left(\frac{2e}{\mathcal{V}_0}\right)^2\Re\Bigg[\sum_{\mathbf{k}}v_{\mathbf{k},\alpha}\sum_{\mathbf{k}'}(i\omega\mathbb{I}+\Lambda)^{-1}_{\mathbf{k}\mathbf{k}'} \times\left(f^s_{\mathbf{k}'}(v_{\mathbf{k}',\beta}-V_\beta)\right)\Bigg], \tag{6}$$

where j_α and j_β are the currents along axes α and β, and $\mathbb{I}$ is the identity matrix. In the limit $\omega\tau \ll 1$, where τ is a characteristic relaxation time, $S_{j_\alpha j_\beta}$ is proportional to the diffusion coefficient, a relation known as the fluctuation-diffusion relation [32]. Therefore, the diffusion coefficient may also be computed from Eq. (6).

In this work, we also computed the piezoresistivity of electrons in Si. For the calculations with compressive stress in the [001] direction, a small uniaxial compressive strain was applied in the [001] direction, and the other two lattice vectors were then relaxed. For the calculations with compressive stress in the [011] direction, the lattice vectors were changed manually until the desired stress state was reached.

The numerical details are as follows. For all calculations, the electronic structure and electron-phonon matrix elements are computed on a coarse $14\times14\times14$ grid using DFT and DFPT with QUANTUM ESPRESSO [33]. This finer coarse grid was used, in comparison to the $8\times8\times8$ [29] that was found to be sufficient to converge the unstressed mobility. A wave-function energy cutoff of 40 Ryd was used for all calculations, and a relaxed lattice parameter of 5.431 Å was used for the unstrained properties. The electronic structure and electron-phonon matrix elements were interpolated onto the fine grid using PERTURBO [34]. For every combination of applied stress value and direction, the electronic structure and electron-phonon matrix elements were recomputed. The piezoresistivity was then computed by calculating the transverse mobility using Eq. (5) from which the resistivity may be obtained, and then normalizing by the calculated unstrained resistivity value.

For temperatures of 160–300 K, a grid density of $100\times100\times100$ for the electron states was used, while a grid density of $50\times50\times50$ was used for the phonons. We report

convergence tests on the PSD values, as they are more sensitive to the details of the band structure and electron-phonon interaction than the mobility. Using a phonon grid with the same density as the electron grid resulted in a PSD change of 17% at 10 kV cm^{-1}, and using a grid density of $120 \times 120 \times 120$ for the electron states and $60 \times 60 \times 60$ for the phonon states resulted in a PSD change of 20% at 10 kV cm^{-1}. The quantity of relevance to our findings is the anisotropy between [111] and [100], defined as $(\mathrm{PSD}_{[111]} - \mathrm{PSD}_{[100]})/\mathrm{PSD}_{[111]}$. This quantity only changed by 0.5% when changing the grid density, indicating that the PSD anisotropy was well converged. From 160–300 K we used an energy window of 284 meV above the conduction-band minimum with a Gaussian smearing parameter of 5 meV, and increasing this energy window to 342 eV resulted in a PSD change at 10 kV cm^{-1} of 1%.

For the grid density at 77 K, a grid density of $140 \times 140 \times 140$ for the electron states and $70 \times 70 \times 70$ for the phonon states was used, with an energy window of 145 meV and a Gaussian smearing parameter of 2.5 meV. For 77 K, increasing the energy window to 284 meV resulted in a PSD change of 7% at 1 kV cm^{-1}. Using a phonon grid with the same density as the electron grid resulted in a change of 12% in the PSD at 1 kV cm^{-1}, the largest field used. Using a grid density of $160 \times 160 \times 160$ for the electron states and $80 \times 80 \times 80$ for the phonon states resulted in a PSD change of 18% at 1 kV cm^{-1}. However, as before, our findings are not affected by these changes, as the qualitative trend of the PSD compared to experiment is unchanged, and the sign of the anisotropy is unchanged. Therefore, the calculations are converged adequately at 77 K for the PSD.

For the piezoresistivity calculations (all performed in the low-field limit), a grid density of $400 \times 400 \times 400$ ($200 \times 200 \times 200$) for electrons (phonons) was required. Increasing the electron grid density to $500 \times 500 \times 500$ and the phonon grid to $250 \times 250 \times 250$ resulted in mobility changes of 15%. The relevant quantity for our conclusions is the piezoresistivity, which is normalized by the zero-stress resistivity value, and the normalized values changed only on the order of 5%. In this case, an energy window of 20 meV was employed for computational tractability. Increasing the energy window from 20 meV to 25 meV resulted in mobility changes of 4%.

The final linear system of equations used to obtain the mobility and the PSD was then solved by a Python implementation of the GMRES method [35]. For all calculations and temperatures, the Fermi level was adjusted to yield a carrier density of 4×10^{13} cm^{-3}. Spin-orbit coupling was neglected, as it has a weak effect on electron transport properties in Si [3,36]. Similarly, quadrupole electron-phonon interactions were neglected [37]. For all calculations of the diffusion coefficient, a frequency of 1 GHz was used, selected to ensure that $\omega\tau^{-1} \ll 1$, where τ is a characteristic relaxation time, while avoiding too low frequencies which result in numerical instabilities.

In our past work [29], it has been shown that two-phonon scattering (2ph) is non-negligible in n-Si. Thus, for all PSD calculations, two-phonon scattering was included. For the piezoresistivity calculations, 2ph scattering could not be included due to the computational cost. However, we do not expect the absence of 2ph scattering for piezoresistivity to affect our conclusions, as it was shown in Ref. [29] that the energy dependence of 2ph scattering rates exhibited the same qualitative trends as those of one-phonon rates, and further that most of the effect of 2ph scattering can be accounted for by scaling the 1ph scattering rates. As this scaling would be present at all applied stresses, we therefore do not expect that neglecting 2ph would affect the piezoresistivity values and our conclusions.

III. RESULTS

A. Electric-field dependence of hot electron diffusion coefficient

We begin by examining the dependence of the diffusion coefficient on electric field at various temperatures. We first compare the experimental low-field values of the diffusion coefficient to the computed ones. We considered four temperatures (300, 200, 160, and 77 K), corresponding to those for which experimental data is available. At these temperatures, the computed (experimental) diffusion coefficients were 29.7 (37) cm^{2}s^{-1}, 59.3 (62) cm^{2}s^{-1}, 58.8 (71) cm^{2}s^{-1}, and 1120 (141) cm^{2}s^{-1}. For all temperatures besides 77 K, the computation underestimates the experimental data. The magnitude of the underestimate for $T > 77$ K is consistent with a prior calculation of the electron mobility of Si when two-phonon scattering is included [29]. However, at 77 K, the computed value is $\sim 8\times$ larger than experiment. This overestimate is possibly attributable to ionized impurity scattering which is neglected in the present calculations.

To facilitate the comparison of trends with electric field in the subsequent plots, the computed data has been normalized to the calculated low-field diffusion coefficient, while the experimental data has been normalized to the value at the lowest electric field reported. We note that due to the requirement that the transit time in the time-of-flight experiment be less than the dielectric relaxation time, no data was reported below a minimum field at each temperature [14]. The electric-field dependence of the diffusion coefficient at 300 K is shown in Fig. 1(a). In experiment, it is observed that at low fields, the diffusion coefficient along the [100] and [111] directions are equal. Starting at less than 2 kV cm^{-1}, the diffusion coefficient along the [111] direction is less than in the [100], an anisotropy that has been attributed to intervalley diffusion [14]. The magnitude of this anisotropy continues to increase with field, reaches a maximum, and then decreases with field. The same qualitative trend with field is seen at 200 K in Fig. 1(b), with the main difference being the anisotropy manifesting at lower fields than at higher temperatures. At 160 K, shown in Fig. 1(c), there is a slight peak of the diffusion coefficient in the [100] direction at low fields and then a monotonic decrease for higher fields. At 77 K, shown in Fig. 1(d), initial increases of the diffusion coefficient with field are seen for both directions.

The calculated results generally predict these trends qualitatively. At 300 K and 200 K, the correct trend of the anisotropy is reproduced, as the [111] diffusion coefficient is less than the [100] value once field values exceed 5 kV cm^{-1} and 2 kV cm^{-1}, respectively. While the initial increase seen in experiment at 160 K with field applied in the [100] direction is not captured by computation, the qualitative anisotropy at high fields is reproduced. Similarly, at 77 K, the [111]

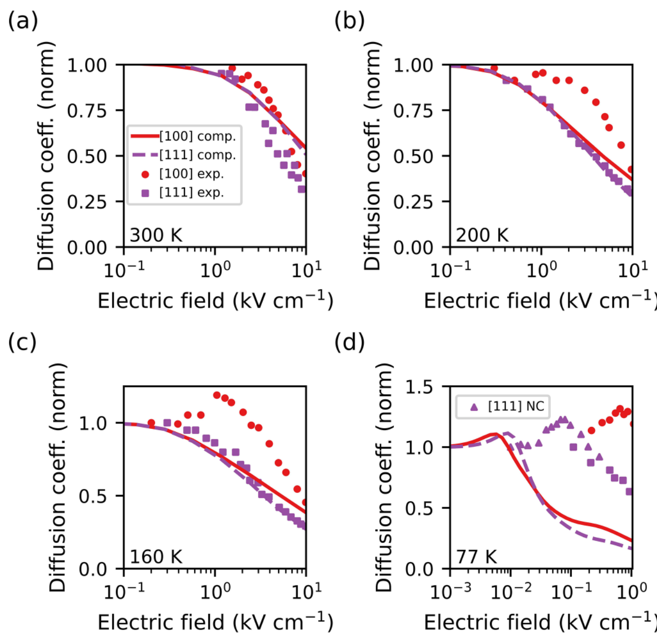

FIG. 1. Normalized diffusion coefficient versus electric field at (a) 300 K, (b) 200 K, (c) 160 K, and (d) 77 K, with field applied along the [100] direction (red solid line) and [111] direction (purple dashed line). Experimental data along the [100] direction (red circles) and [111] direction (purple squares) from Figs. 3 and 4, Ref. [14]. In (d), noise conductivity (NC) measurements (purple triangles) included for comparison at low electric fields.

diffusion coefficient is less than in the [100] once the electric field exceeds 0.2 kV cm^{-1}.

However, a number of quantitative discrepancies can be seen. At 160, 200, and 300 K, the computed anisotropy starts to manifest at higher fields than in experiment. In experiment, at 300 K the anisotropy is observed once the electric field exceeds 2 kV cm^{-1}, while at 200 K and 160 K the anisotropy manifests even below 1 kV cm^{-1}. Similarly, the magnitude of the anisotropy is underestimated, particularly for 160 K and 200 K, where the agreement with the [111] data is excellent, but the [100] data lies much above the computed values.

At 77 K, the qualitative behavior of the diffusion coefficient with field changes greatly. We note that the electric-field range used in this calculation is smaller than in the other cases due to lack of convergence at high fields. In Fig. 1(d), in both directions measured an initial increase in the experimental PSD is seen. This increase is observed in computation, but at lower fields than in experiment. Given the relative importance of ionized impurity scattering at 77 K compared to higher temperatures, we examined whether the omission of this scattering mechanism in the calculation could play a role in the discrepancy. We implemented a simple model of ionized impurity scattering [38] with a density of 10^{14} cm^{-3}. The nonmonotonic features were observed to shift to higher electric fields, suggesting that ionized impurity scattering could be partly responsible for this discrepancy.

The anisotropy in the diffusion coefficient seen in experiment has been attributed to a mechanism known as intervalley diffusion. [14] To understand this mechanism, consider the general expression for the intervalley diffusion coefficient D^{int}, given by $D^{\text{int}} = n_1 n_2 (v_1 - v_2)^2 \tau_{\text{int}}$. [12,14] Here, n_1 and n_2 are the fractions of electrons in valleys of type 1 and 2, v_1 and v_2 are the drift velocities in valleys of type 1 and 2, and τ_i is the characteristic intervalley relaxation time. When the field is applied in the [111], the average velocities in each valley type are equal, and this extra contribution vanishes. While many transport properties such as mobility are insensitive to the balance between g- (between equivalent valleys) and f-type (between inequivalent valleys) scattering, τ_{int} is inversely proportional to the square of the f-type coupling constant [14]. A possible origin of the underpredicted anisotropy in the diffusion coefficient is therefore computed f-type scattering rates which are too large compared to experiment. To test this hypothesis, we compute other transport and noise properties which are sensitive to the distinct types of intervalley scattering.

B. Microwave-frequency PSD

We first compute the microwave frequency ($\sim$0.1–100 GHz) PSD at 77 K and 200 V cm^{-1}, for which experimental data is available for comparison [15]. Here, the frequency ranges computed are much higher than those in which sources of noise such as $1/f$ noise or generation-recombination noise would be relevant. However, if the frequency is comparable to an inverse time constant τ such as the momentum or energy relaxation time, nonmonotonic features or rolloffs in the PSD with increasing frequency around frequencies satisfying $\omega\tau \sim 1$ will be observed [10]. Comparing the frequencies at which these features occur therefore provides an independent test of the accuracy of the *ab initio* diffusion coefficient calculations.

Figure 2 shows the calculated spectral density of current fluctuations versus frequency, at 77 K and 200 V cm^{-1} and with electric fields applied along the [111] and [100] directions, along with experimental data. At frequencies below 3 GHz, the [100] PSD is greater than the [111], due to the presence of intervalley diffusion. As intervalley scattering is characterized by a significantly smaller relaxation rate than either the energy or momentum relaxation rates, a rolloff in the [100] direction is observed around the relatively low frequency of 1 GHz. The presence of the “convective” mechanism away from equilibrium rolls off at a frequency corresponding to the energy relaxation rate. Here, the convective peak occurs around 25 GHz. For semiconductors with a sublinear current-voltage characteristic, this convective contribution is negative [10]. This mechanism is present in both the [100] and [111] cases, but is more obviously present in the [111] due to the lack of intervalley noise. Finally, as the frequency exceeds the momentum relaxation rate, the PSD rolls off to zero as the electronic system is not able to redistribute in response to the oscillating external field.

Over the entire calculated frequency range, the computed results qualitatively capture the trends seen in experiment. The anisotropy seen at low frequencies due to intervalley noise, the rolloff in the [100] direction starting around 1 GHz due to frequency exceeding the characteristic intervalley scattering rate, and the convective noise peaks are all reproduced. At frequencies above 100 GHz, the PSD is higher in the [111] direction, simply due to the greater mobility in this direction

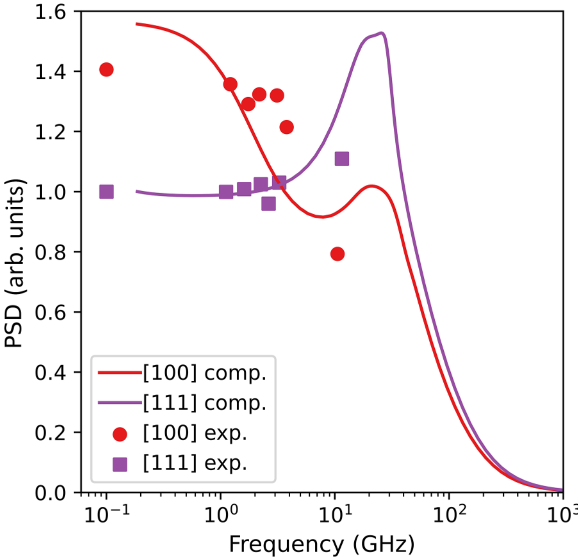

FIG. 2. Microwave PSD versus frequency at 77 K and 200 V cm^{-1} applied electric field, with field applied along the [100] direction (red solid line) and [111] direction (purple solid line). Experimental data along the [100] direction (red circles) and [111] direction (purple squares) from Fig. 1, Ref. [15]. In both cases, the data is normalized to the value of the PSD at the lowest-frequency data point (computation, 0.19 GHz; experiment, 0.1 GHz) in the [111] direction.

at 200 V cm^{-1}. Relaxation times for the various noise sources (thermal, convective, and intervalley) can be obtained by fitting the computed curves to Lorentzians parameterized by the various relaxation times, as given in Eq. (9.5) in Ref. [10]. For the [111] direction, an energy relaxation time of 15 ps was calculated using Monte Carlo simulation, as well as a momentum relaxation time of 2 ps, while our computation yields an energy relaxation time of 9 ps, and a momentum relaxation time of 4 ps [10]. For the [100] direction, Monte Carlo simulation reported an energy relaxation time of 5 ps [10], and an intervalley relaxation time of 50 ps [15], while our computation yields an energy relaxation time of 10 ps, and an intervalley relaxation time of 79 ps. The magnitudes of the relaxation times and relative difference between the momentum and energy relaxation times are thus in qualitative agreement with prior works. However, data only exists up to intermediate frequencies (around 10 GHz), so it is difficult to draw quantitative conclusions, especially for the momentum relaxation time.

As the difference in the PSD at low frequency is due to intervalley noise, and the magnitude of this difference is captured accurately by our computation, the results of Fig. 2 suggest that the f-type scattering rates in computation are compatible with their actual values. In addition, the frequency of the intervalley rolloff and convective mechanism being well captured imply that both the intervalley and energy relaxation rates are qualitatively consistent with experimental values.

C. Piezoresistivity

We next compute the piezoresistivity at 300 K and 77 K, for which experimental data is available [39]. Piezoresistivity

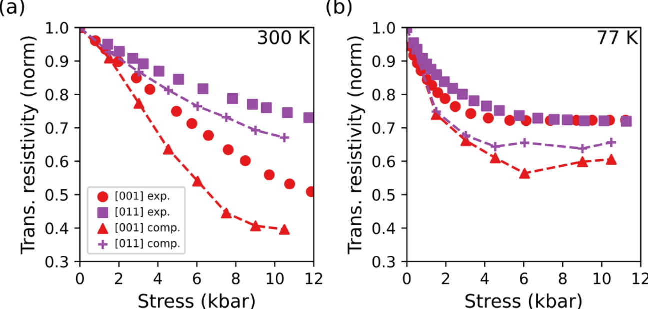

FIG. 3. Computed normalized transverse resistivity versus stress at (a) 300 K and (b) 77 K, with stress applied along the [001] direction (red triangles) and [011] direction (purple crosses). Experimental data along the [001] direction (red circles) and [011] direction (purple squares) from Figs. 3 and 4, Ref. [39].

provides information about f-type intervalley scattering due to the following considerations. When compressive stress is applied along a crystallographic direction, valleys parallel to the stress axis decrease in energy compared to the other valleys. Therefore, if the stress is applied in the [001] direction, in the limit of high stress all electrons will be in the [001] valleys. Similarly, if stress is applied in the [011] direction, electrons will be in the [010] and [001] valleys. In the first case ([001] stress), all f-type scattering will be eliminated. However, in the second case ([011] stress), f-type intervalley scattering between [010] and [001] valleys remains. Therefore, if f-type scattering is negligible [such as at 77 K as seen in experiment in Fig. 3(b)], the transverse resistivity (for instance resistivity measured along [100]) at high stress in both cases is expected to be identical [40]. If f-type scattering is present [as at 300 K as seen in experiment in Fig. 3(a)], the case with the stress oriented along the [001] will have a lower resistivity due to the lack of f-type scattering.

In Fig. 3(a), the computed transverse resistivity versus stress in the [001] and [011] directions at 300 K is presented. The computed anisotropy exhibits qualitative agreement with experiment, as in both cases the resistivity is less when the stress is applied along the [001] compared to the [011] case. Due to the non-negligible contribution of f-type scattering at 300 K, applying pressure along the [001] eliminates f-type scattering in the high-stress limit and thereby decreases the resistivity by a greater amount than in the [011] case. However, the computation underpredicts the transverse resistivity at all pressures for both applied stress directions.

In Fig. 3(b), the computed transverse resistivity versus stress at 77 K is shown along with experimental data. Here, it is observed in experiment that at high stresses, the resistivity along both directions saturates to closer to the same value than at 300 K. The computed resistivity saturates with pressure to a slightly lower value than in experiment, but the difference between the two directions is considerably smaller than at 300 K (69% at 300 K versus 8% at 77 K). The relatively small difference in the high-pressure 77 K resistivity between the two directions indicates that f-type scattering is negligible at this temperature, while at 300 K the computed difference between the two directions is comparable with experimental results. The agreement at both temperatures indicates that the

magnitude of f-type scattering at these temperatures is being qualitatively captured.

IV. DISCUSSION

Figure 1 indicates that the anisotropy of the diffusion coefficient in n-Si is qualitatively captured in the calculation, with the diffusion coefficient in the [111] direction being less than in the [100] in the high-field limit for all temperatures measured. The primary discrepancies between experiment and computation between 160 and 300 K are the anisotropy in the computed results being smaller and not manifesting until higher fields compared to experiment. The smaller anisotropy in the computed results suggests that the computation underestimates the amount of intervalley noise, and thus overestimates the amount of f-type scattering. However, Fig. 2 indicates that the computed intervalley scattering rates and intervalley noise magnitude are qualitatively compatible with experiment, and Fig. 3 shows that the variation of f-type scattering with temperature is qualitatively captured as well. The amount of error in the computed f-type scattering rate is therefore constrained to values that are insufficient to explain the discrepancies in the diffusion coefficient.

Given these observations, and that we have used the highest level of *ab initio* theory presently available which includes two-phonon scattering, our findings suggest an external mechanism not contained in the computation is responsible for the discrepancy. We suggest that this mechanism could be the neglect of spatial inhomogeneities present in experiment. The *ab initio* method used here does not include real-space effects such as concentration gradients or space-charge effects. Although the time-of-flight experiment was carefully implemented to avoid dielectric relaxation in the sample, it is conceivable that fluctuations in drift velocity associated with intervalley scattering within the generated electron pulse could lead to space-charge effects which would spatially broaden the pulse and hence increase the measured diffusion coefficient. This effect would be present only in the [100] direction due to the absence of intervalley scattering in the [111] direction. Further, these effects would not appear in the microwave PSD as these frequencies are much higher than those associated with any dielectric relaxation phenomena. Additional study will be required to determine the origin of the diffusion coefficient discrepancies.

V. SUMMARY

We have computed the hot electron diffusion coefficient, microwave PSD, and piezoresistivity in Si from first principles from 77–300 K. We find that while qualitative features of the diffusion coefficient such as the anisotropy at high electric fields are generally predicted, several trends of the calculated values differ from experiment. We computed the piezoresistivity and microwave PSD to investigate whether an inaccurate description of f-type intervalley scattering could explain the discrepancies. However, the good qualitative agreement of these properties with experiment excluded this possibility, leading to the hypothesis that the measured diffusion coefficient is influenced by factors not included in *ab initio* calculations such as real-space gradients and space-charge effects. This finding indicates that care must be taken when interpreting diffusion coefficient measurements in terms of microscopic charge transport processes.

ACKNOWLEDGMENTS

B.H. was supported by a NASA Space Technology Graduate Research Opportunity under Grant No. 80NSSC21K1280. A.J.M. was supported by AFOSR under Grant No. FA9550-19-1-0321. The authors thank J. Sun, S. Sun, D. Catherall, and T. Esho for helpful discussions.

[1] W. Li, Electrical transport limited by electron-phonon coupling from Boltzmann transport equation: An *ab initio* study of Si, Al, and MoS_2, Phys. Rev. B **92**, 075405 (2015).
[2] M. Fiorentini and N. Bonini, Thermoelectric coefficients of n-doped silicon from first principles via the solution of the Boltzmann transport equation, Phys. Rev. B **94**, 085204 (2016).
[3] S. Poncé, E. R. Margine, and F. Giustino, Towards predictive many-body calculations of phonon-limited carrier mobilities in semiconductors, Phys. Rev. B **97**, 121201(R) (2018).
[4] J.-J. Zhou and M. Bernardi, *Ab initio* electron mobility and polar phonon scattering in GaAs, Phys. Rev. B **94**, 201201(R) (2016).
[5] T.-H. Liu, J. Zhou, B. Liao, D. J. Singh, and G. Chen, First-principles mode-by-mode analysis for electron-phonon scattering channels and mean free path spectra in GaAs, Phys. Rev. B **95**, 075206 (2017).
[6] M. Bernardi, First-principles dynamics of electrons and phonons, Eur. Phys. J. B **89**, 239 (2016).
[7] F. Giustino, Electron-phonon interactions from first principles, Rev. Mod. Phys. **89**, 015003 (2017).
[8] S. Poncé, F. Macheda, E. R. Margine, N. Marzari, N. Bonini, and F. Giustino, First-principles predictions of Hall and drift mobilities in semiconductors, Phys. Rev. Res. **3**, 043022 (2021).
[9] S. Poncé, W. Li, S. Reichardt, and F. Giustino, First-principles calculations of charge carrier mobility and conductivity in bulk semiconductors and two-dimensional materials, Rep. Prog. Phys. **83**, 036501 (2020).
[10] H. L. Hartnagel, R. Katilius, and A. Matulionis, *Microwave Noise in Semiconductor Devices* (John Wiley & Sons, New York, 2001), Chap. 8.
[11] E. Conwell, *High Field Transport in Semiconductors* (Academic Press, New York, 1967).
[12] P. J. Price, Intervalley noise, J. Appl. Phys. **31**, 949 (1960).
[13] C. Canali, C. Jacoboni, G. Ottaviani, and A. Alberigi-Quaranta, High-field diffusion of electrons in silicon, Appl. Phys. Lett. **27**, 278 (1975).
[14] R. Brunetti, C. Jacoboni, F. Nava, L. Reggiani, G. Bosman, and R. J. J. Zijlstra, Diffusion coefficient of electrons in silicon, J. Appl. Phys. **52**, 6713 (1981).

[15] V. Bareĭkis, V. Viktoravichyus, and A. Gal'dikas, Frequency dependence of noise in *n*-type Si in high electric fields, Fiz. Tekh. Poluprovodn. **16**, 1868 (1982) [Sov. Phys. Semicond. **16**, 1202 (1982)].
[16] C. Jacoboni, R. Minder, and G. Majni, Effects of band non-parabolicity on electron drift velocity in silicon above room temperature, J. Phys. Chem. Solids **36**, 1129 (1975).
[17] C. Jacoboni and L. Reggiani, The Monte Carlo method for the solution of charge transport in semiconductors with applications to covalent materials, Rev. Mod. Phys. **55**, 645 (1983).
[18] E. Pop, R. W. Dutton, and K. E. Goodson, Analytic band Monte Carlo model for electron transport in Si including acoustic and optical phonon dispersion, J. Appl. Phys. **96**, 4998 (2004).
[19] Z. Aksamija and U. Ravaioli, Joule heating and phonon transport in silicon mosfets, J. Comput. Electron. **5**, 431 (2006).
[20] M. V. Fischetti, Monte Carlo simulation of transport in technologically significant semiconductors of the diamond and zinc-blende structures. I. homogeneous transport, IEEE Trans. Electron Devices **38**, 634 (1991).
[21] B. Fischer and K. R. Hofmann, A full-band Monte Carlo model for the temperature dependence of electron and hole transport in silicon, Appl. Phys. Lett. **76**, 583 (2000).
[22] P. H. Nguyen, K. R. Hofmann, and G. Paasch, Comparative full-band Monte Carlo study of Si and Ge with screened pseudopotential-based phonon scattering rates, J. Appl. Phys. **94**, 375 (2003).
[23] M. V. Fischetti, P. D. Yoder, M. M. Khatami, G. Gaddemane, and M. L. Van de Put, "Hot electrons in Si lose energy mostly to optical phonons": Truth or myth? Appl. Phys. Lett. **114**, 222104 (2019).
[24] A. Y. Choi, P. S. Cheng, B. Hatanpää, and A. J. Minnich, Electronic noise of warm electrons in semiconductors from first principles, Phys. Rev. Mater. **5**, 044603 (2021).
[25] I. Maliyov, J. Park, and M. Bernardi, Ab initio electron dynamics in high electric fields: Accurate prediction of velocity-field curves, Phys. Rev. B **104**, L100303 (2021).
[26] P. S. Cheng, J. Sun, S.-N. Sun, A. Y. Choi, and A. J. Minnich, High-field transport and hot-electron noise in GaAs from first-principles calculations: Role of two-phonon scattering, Phys. Rev. B **106**, 245201 (2022).
[27] J. Sun and A. J. Minnich, Transport and noise of hot electrons in GaAs using a semianalytical model of two-phonon polar optical phonon scattering, Phys. Rev. B **107**, 205201 (2023).
[28] D. S. Catherall and A. J. Minnich, High-field charge transport and noise in *p*-Si from first principles, Phys. Rev. B **107**, 035201 (2023).
[29] B. Hatanpää, A. Y. Choi, P. S. Cheng, and A. J. Minnich, Two-phonon scattering in nonpolar semiconductors: A first-principles study of warm electron transport in Si, Phys. Rev. B **107**, L041110 (2023).
[30] A. A. Mostofi, J. R. Yates, Y.-S. Lee, I. Souza, D. Vanderbilt, and N. Marzari, wannier90: A tool for obtaining maximally-localised Wannier functions, Comput. Phys. Commun. **178**, 685 (2008).
[31] N. Marzari, A. A. Mostofi, J. R. Yates, I. Souza, and D. Vanderbilt, Maximally localized Wannier functions: Theory and applications, Rev. Mod. Phys. **84**, 1419 (2012).
[32] S. V. Gantsevich, V. L. Gurevich, and R. Katilius, Theory of fluctuations in nonequilibrium electron gas, Riv. Nuovo Cimento **2**, 1 (1979).
[33] P. Giannozzi, S. Baroni, N. Bonini, M. Calandra, R. Car, C. Cavazzoni, D. Ceresoli, G. L. Chiarotti, M. Cococcioni, I. Dabo, A. Dal Corso, S. De Gironcoli, S. Fabris, G. Fratesi, R. Gebauer, U. Gerstmann, C. Gougoussis, A. Kokalj, M. Lazzeri, L. Martin-Samos *et al.*, QUANTUM ESPRESSO: A modular and open-source software project for quantum simulations of materials, J. Phys.: Condens. Matter **21**, 395502 (2009).
[34] J.-J. Zhou, J. Park, I. Lu, I. Maliyov, X. Tong, and M. Bernardi, Perturbo: A software package for *ab initio* electron-phonon interactions, charge transport and ultrafast dynamics, Comput. Phys. Commun. **264**, 107970 (2021).
[35] V. Frayssé, L. Giraud, S. Gratton, and J. Langou, Algorithm 842: A set of GMRES routines for real and complex arithmetics on high performance computers, ACM Trans. Math. Softw. **31**, 228 (2005).
[36] J. Ma, A. S. Nissimagoudar, and W. Li, First-principles study of electron and hole mobilities of Si and GaAs, Phys. Rev. B **97**, 045201 (2018).
[37] J. Park, J.-J. Zhou, V. A. Jhalani, C. E. Dreyer, and M. Bernardi, Long-range quadrupole electron-phonon interaction from first principles, Phys. Rev. B **102**, 125203 (2020).
[38] D. Long and J. Myers, Ionized-impurity scattering mobility of electrons in silicon, Phys. Rev. **115**, 1107 (1959).
[39] K. V. Hansen, Some investigations of the intervalley scattering in N-type silicon, Ph.D. thesis, Technical University of Denmark, 1974.
[40] M. H. Jørgensen, Electron-phonon scattering and high-field transport in *n*-type Si, Phys. Rev. B **18**, 5657 (1978).